Thin Solid Films 519 (2011) 6224–6229

Contents lists available at ScienceDirect

Thin Solid Films

journal homepage: www.elsevier.com/locate/tsf

Superhydrophobic transparent films from silica powder: Comparison of fabrication methods

Li-Der Liu [a], Chao-Sung Lin [a,*], Mukul Tikekar [b], Ping-Hei Chen [c]

[a] Department of Material Science and Engineering, National Taiwan University, Taipei, Taiwan
[b] Department of Mechanical Engineering, Indian Institute of Technology-Bombay, Bombay, India
[c] Department of Mechanical Engineering, National Taiwan University, Taipei, Taiwan

ARTICLE INFO

Article history:
Received 1 February 2010
Received in revised form 23 March 2011
Accepted 23 March 2011
Available online 6 April 2011

Keywords:
Self-cleaning surfaces
Superhydrophobicity
Transmissivity
Sol–gel deposition
Silica
Polydimethylsiloxane

ABSTRACT

The lotus leaf is known for its self-clean, superhydrophobic surface, which displays a hierarchical structure covered with a thin wax-like material. In this study, three fabrication techniques, using silicon dioxide particles to create surface roughness followed by a surface modification with a film of polydimethylsiloxane, were applied on a transparent glass substrate. The fabrication techniques differed mainly on the deposition of silicon dioxide particles, which included organic, inorganic, and physical methods. Each technique was used to coat three samples of varying particle load. The surface of each sample was evaluated with contact angle goniometer and optical spectrometer. Results confirmed the inverse relationships between contact angle and optical transmissivity independent of fabrication techniques. Microstructural morphologies also suggested the advantage of physical deposition over chemical methods. In summary, the direct sintering method proved outstanding for its contact angle vs transmissivity efficiency, and capable of generating a contact angle as high as 174°.

1. Introduction

Many studies refer to the surface structure of lotus leaves for its water repelling properties. They share a rough surface consisting of micro- and nanostructures. In addition, the surface of these structures is made of a wax-like material with surface energies much lower than water. As water comes in contact with such a surface structure, most dirt particles are wetted preferentially and carried off the surface. Thus, the primary objective to bio-mimic a superhydrophobic self-clean surface is to produce a desirable surface roughness with reduced surface energy. However, surface roughness has been reported to compromise the optical transmissivity due to scattering in the optical wavelengths [1]. Recently, Ling et al. [2] and Yanagisawa et al. [3] have separately reported, in 2009, ways of pushing the limit of such an effect by introducing a delicate nano-scale roughness. Paz et al. [4,5], Roméas et al. [6], and others have also provided reports on fully transparent photocatalytic methods towards self-clean surface solutions. In this study, the fabrication of transparent self-clean treatments is focused specifically on building superhydrophobic surface structures.

There is a wide variety of particle deposition methods available for producing surface roughness microstructures, including electrochemical [7,8], electroless [9–12], electrospinning [13], plasma [14], RFD [15], sintering [2], template [16–21], UV cure [22], and other sol–gel fabrications in general [3,23–39]. Numerous literatures reported surface modified superhydrophobicity [2,3,10,12–14,16–18,21,23,24,26–28,30,33,40–50]. A number of surface structures are potentially highly transparent [11–13,15,19,21,26,31,40,47,51]. The purpose of this study is to extend such fabrication techniques reported that were performed with opaque materials or opaque substrates, that involved expansive equipments and high temperature process (>700 °C) incompatible with ordinary window glass, that required special substrate material or sample scales that were unsuitable for process industrialization, to a fabrication method compatible with ordinary window glass at reasonable costs. The transparent self-clean material is intended for outdoor solar panels and LED covers. The fabrication methods explored involved three techniques, each using a combination of nano-sized round silicon dioxide particles to create robust surface roughness with a surface modification of polydimethylsiloxane (PDMS), on transparent glass substrates. The fabrication techniques differed mainly on the deposition of silicon dioxide particles, which included organic, inorganic, and physical methods. Each technique was used to coat three samples of varying particle load. The surfaces of each sample were evaluated by contact angle, optical transmissivity, and ASTM D3363 pencil hardness test [52].

2. Experimental details

The materials selected for surface roughness are silicon dioxide particles due to its transparent optical properties, superior wear resistance properties, and UV stable properties over polymeric materials.

* Corresponding author. Tel.: +886 2 33665240; fax: +886 2 23634562.
E-mail address: csclin@ntu.edu.tw (C.-S. Lin).

0040-6090/$ – see front matter
doi:10.1016/j.tsf.2011.03.129

Two different sources of silica powder were used. In the organic technique, uniform spherical nano-silica of 50 nm in diameter were synthesised and attached to micro-silica of 1 μm as shown in Fig. 1(a). The synthesis of such particles refers to the well-known Stöber method [27,53,54]. The surface of nano-silica synthesised was reacted with 3-Aminopropyl triethoxysilane (APS) to form a surface of $-NH_2$ radicals, whilst the surface of micro-silica synthesised was reacted with 3-Glycidoxypropyl trimethoxysilane to form a surface of epoxide radicals [27]. Mixed in a bath of ethanol solution, the nano-silica attaches itself to the micro-silica forming a hierarchical silica structure. In the inorganic and physical fabrication techniques, commercial silica particles with an average diameter of 40 nm were purchased. A scanning electron microscope image of such particles was taken and shown in Fig. 1(b). Details on the particle deposition are described in the following subsections, including a final coat of non-polar water repelling PDMS or phenyltrimethysilane on the rough surface.

2.1. Organic attachment

The hierarchical silica microstructural roughness consisted of nano-scaled silica spheres attached on the surface of micron-sized silica spheres. The silica spheres were produced according to Stöber's sol–gel method according to Ming's recipe [27]. The precursor chemical was tetraethoxysilane (TEOS), reacted in a solution containing organic solvents including methanol, ethanol, and isopropanol with the addition of ammonia solution as the basic reaction catalyst. The hybrid-sized silica spheres were attached to each other and to the glass slide substrate via reaction between amine and epoxy end groups on the surface of silica spheres. Similar end group reactions were used to produce a final coat of PDMS on the outer surface of the silica hierarchical structures as the final coat [13]. The specific chemicals used to form the epoxy resin on the glass substrate consisted of Trimethylolpropane triglycidyl ether and Poly(Propylene glycol) Bis(2-Aminopropyl ether) (Jeffamine D-230). Nano-silica particles covered the surface of micro-silica particles and exposed $-NH_2$ radicals on the surface to adhere on the epoxy resin on the substrate. The resultant surface structure contained both $-NH_2$ groups and unreacted epoxide groups. Thus, all surface radicals were converted to $-NH_2$ end groups via reacting with Poly(Dimethylsiloxane), Bis(3-Aminopropyl) terminated (n ~ 2500) before a final reaction with Poly(Dimethylsiloxane), Monoglycidal ether terminated (n ~ 5000) (MGE-PDMS).

The processing steps above are illustrated in a graphical representation shown in Fig. 2a with detailed molecular structure and linking reactions illustrated in Fig. 3b. Three samples were produced via this technique with increasing particle loads: RB-1, RB-2, and RB-3 (RB for chemical radical bonding).

2.2. Inorganic route

All chemicals were purchased from Sigma-Aldrich & Co., and used as received. Millipore deionized water was used to prepare the

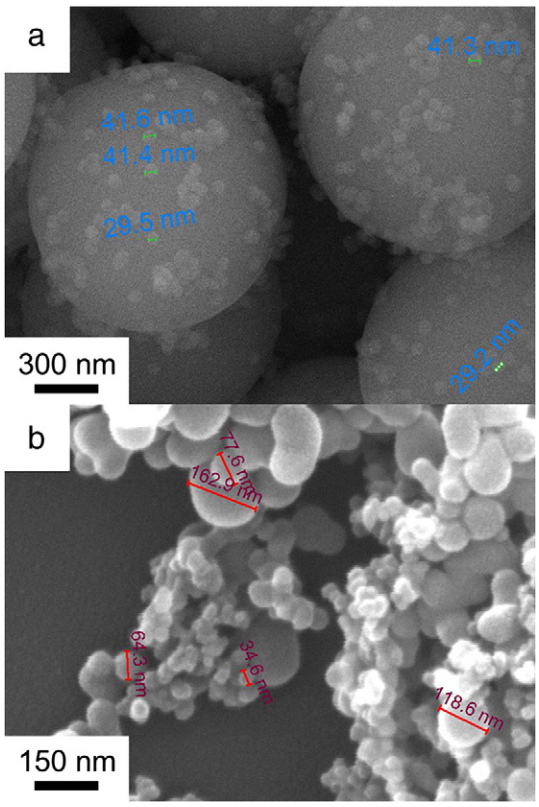

Fig. 1. Silica powder used in (a) organic attachment, (b) inorganic route, and physical binding methods.

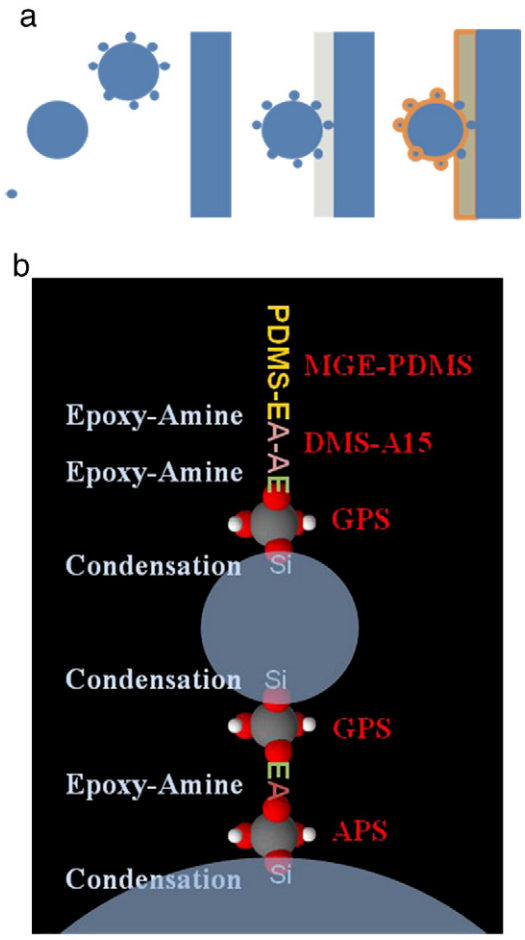

Fig. 2. a. Processing steps in organic attachment method proceeding from left to right. Solid blue indicates bulk silica/glass substrate, transparent blue indicates bonding medium, and orange outlines indicate water repellent surface chemistry. b. Detailed chemical reactions between water repellent molecules, silica particles, and coupling agents. The blue labels on the left column indicate the linking reactions that took place. The red labels on the right column indicate the precursor chemicals before linking reactions took place. In the molecular diagram, the silica particle(s) (transparent blue circles) and representation of the linked molecular structures are not drawn to scale. (-PDMS indicates PDMS end-group, -A indicates amino end-group, -E indicates epoxy end-group, and -A and -E react to form linkage; the grey, red, and white 3-D spheres represent silicon, oxygen, and hydrogen atoms respectively.)

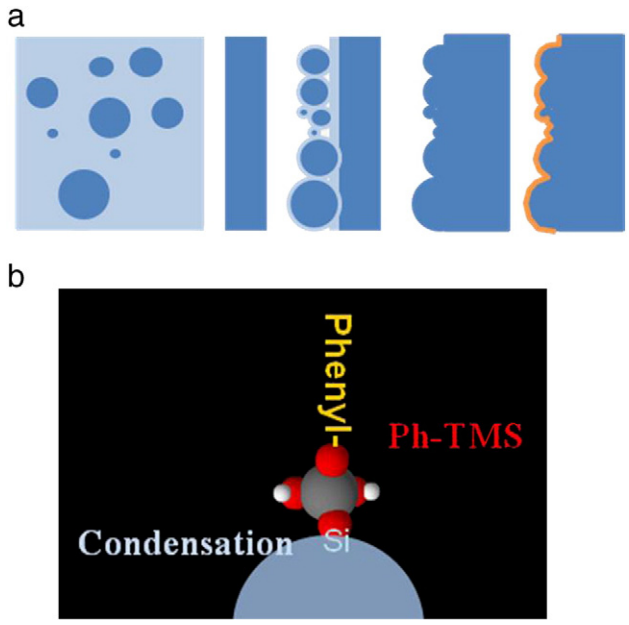

Fig. 3. a. Processing steps of the inorganic route proceeding from left to right. Solid blue indicates bulk silica/glass substrate, transparent blue indicates bonding medium, and orange outline indicates water repellent surface chemistry. b. Detailed chemical reactions between water repellent molecules and silica particles. The blue labels on the left column indicate the linking reactions that took place. The red labels on the right column indicate the precursor chemicals before linking reactions took place. In the molecular diagram, the silica particle(s) (transparent blue circles) and representation of the linked molecular structures are not drawn to scale. (-Phenyl indicate phenyl-end-group; the grey, red, and white 3-D spheres represent silicon, oxygen, and hydrogen atoms respectively.)

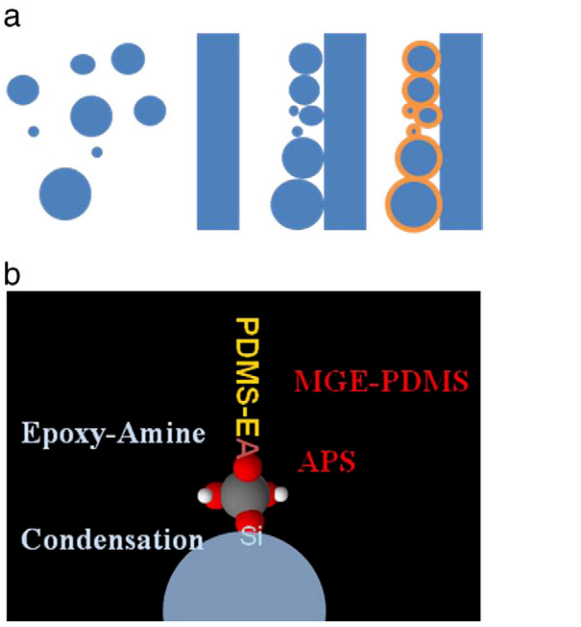

Fig. 4. a. Processing steps of the physical binding method proceeding from left to right. Solid blue indicates bulk silica/glass substrate and orange outline indicates water repellent surface chemistry. b. Detailed chemical reactions between water repellent molecules, coupling agents, and silica particles. The blue labels on the left column indicate the linking reactions that took place. The red labels on the right column indicate the precursor chemicals before linking reactions took place. In the molecular diagram, the silica particle(s) (transparent blue circles) and representation of the linked molecular structures are not drawn to scale. (-Phenyl indicate phenyl-end-group; the grey, red, and white 3-D spheres represent silicon, oxygen, and hydrogen atoms respectively.)

suspensions. TEOS, ethanol, and deionized water were mixed in a 1:4:20 M ratio. The mixture was stirred evenly, using a magnetic stirrer. A few drops of concentrated hydrochloric acid were added to modify the pH value below the isoelectric point (IEP) of silica (pH = 2) as the reaction catalyst. The mixture was then stirred until it was completely miscible. Silica particles were then added to the solution in increasing weight concentrations: SG-1, SG-2, and SG-3 (SG for sol–gel curing). This formed the suspension with which the glass surface was coated. The coated surface was first dried at 80 °C for 40 min in an oven then baked at 200 °C for 90 min. A rough surface has now generated on the surface by sol–gel curing. To further react a non-polar structure on the surface, a solution of phenyltrimethoxysilane in methanol, 5% by weight was prepared. The baked wafers were then immersed in the solution for 8 h. Finally, the wafers were dried at 50 °C for 30 min. A graphical process flow diagram of the sol–gel curing method is shown in Fig. 3a with detailed molecular links illustrated in Fig. 5b.

2.3. Physical binding

Similarly, three particle loads of surface deposition were made: DS-1, DS-2, DS-3 (DS for direct sintering). However, the process of direct sintering eliminated the chemical processes required to fix silica particles on the glass substrate. In physical binding, a high temperature diffusional process was utilised at temperatures below 700 °C for a baking time of 4 h. Similar PDMS treatments were followed from organic attachment methods, with slight modifications. Dilute APS solution in organic solvent (ethanol) was used to immerse sintered samples with baking to cover $-NH_2$ radicals on the surface, and then a final reaction with MGE-PDMS to cap off the surface with PDMS end groups. Similar processing flow diagram is shown in Fig. 4a with detailed molecular links illustrated in Fig. 7b.

2.4. Surface evaluation

The surfaces of each sample were evaluated by contact angle and optical transmissivity, each analysed by FTA125 contact angle goniometer and Ocean Optics USB2000 Fibre Optic Spectrometer, respectively. The particles that were synthesised or purchased as seen in Fig. 1 and some of the resulting surface morphologies were observed with a FEI Quanta 200 FEG Scanning Electron Microscope at accelerating voltage of 20 keV. Pencil scratch hardness was evaluated according to ASTM D3363 standards [52] with a Gardco 3363 Pencil Scratch Hardness Tester.

3. Results and discussion

3.1. Particle load

Fig. 5 shows the water droplet images taken with FTA125 contact angle goniometer and their respective optical transmission spectra for organic attachment (RB), inorganic route (SG), and physical binding (DS) fabrication methods from the lightest to the heaviest particle loads. Visually, the samples of varying particle loads for each fabrication method were tuned in a scale whilst kept optically translucent. In Fig. 5 (a), the contact angles for the organic resin attached samples increased from 98°, 126°, to 132°. In Fig. 5(b), the contact angles for the inorganically cured samples increased from 90°, 121°, to 125°. In Fig. 5(c), the contact angles of the directly sintered samples increased from 166°, 172°, to 174°. In contrast, the corresponding optical transmission spectra reduced as particle load was increased. Similar trends marked for the three different fabrication methods. A slight difference in the curvature of optical transmission spectra was observed. At near-UV region, the sol–gel cured and direct sintered samples showed highest absorption. However, the radical bonding samples revealed significant absorption at wavelengths greater than 500 nm.

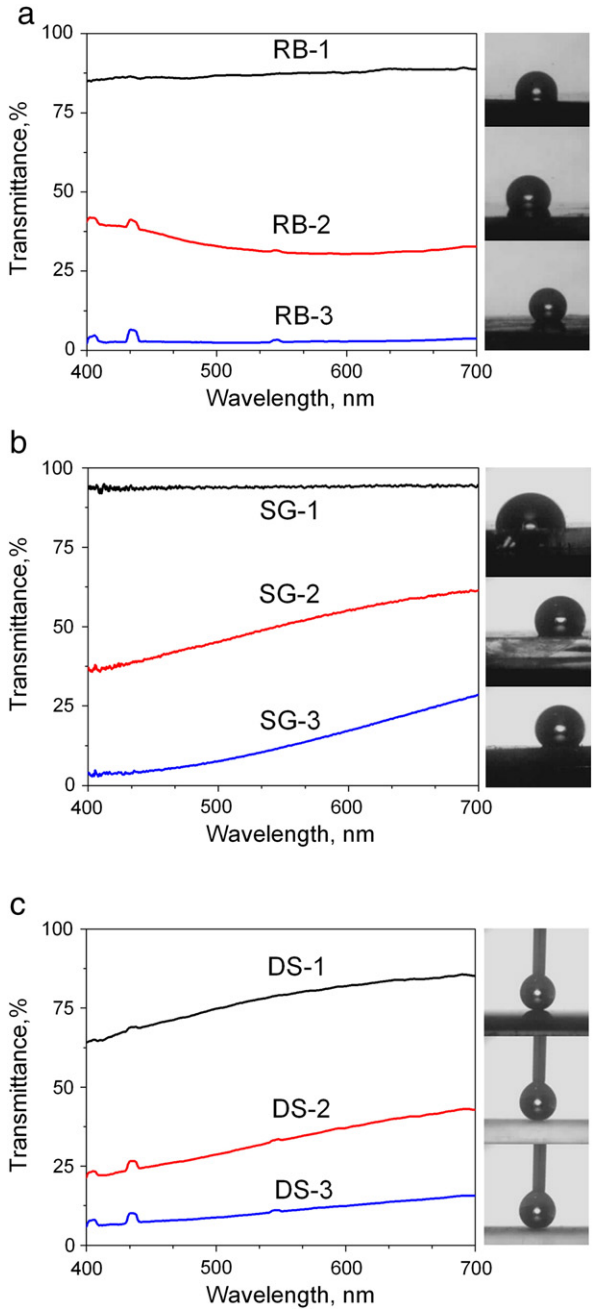

Fig. 5. Contact angles and transmittance spectra in the visible region for (a) organic attachment (RB-1, RB-2, and RB-3), (b) inorganic route (SG-1, SG-2, and SG-3), and (c) physical binding samples (DS-1, DS-2, and DS-3) in increasing particle loads.

This effect is speculated as an indication of particle size due to scattering phenomenon. Moreover, the effect of particle load on the amount of scattering is clear: thicker coating and lower transmitted intensities.

In the three fabrication techniques, the water contact angles increased with heavier particle loads. This indicates a greater surface roughness produced when more particles are deposited. However, the organically attached and inorganically cured techniques failed to achieve superhydrophobicity under the condition of optical transmissivity. A superhydrophobic surface generates a water contact angle of greater than 150° and a roll off angle of less than 5°. RB series achieved a highest 132° whilst SG series achieved a generous 125°. At such contact angles, water droplets easily adsorbed to the surface during contact. A standard 5 μl droplet remained stationary when the samples were tilted up to 5°. However, the samples fabricated with physically sintered methods exhibited properties of superhydrophobicity. At water contact angles of greater than 165°, it was difficult to place a standard 5 μl droplet on the surface of DS-1 without bouncing off the sample surface. On samples DS-2 and DS-3, the water droplet bounced off the surface more freely than DS-1. The surface appeared frictionless against the initial momentum came with placing the water droplet. Given a precision needle tip, it was still almost impossible to place a 5 μl still droplet on a completely levelled surface when contact angles were greater than 170°.

3.2. Efficiency of contact angle vs optical transmittance

The results obtained and averaged from Fig. 5 are plotted in a contact angle vs average optical transmittance graph shown in Fig. 6. From Fig. 6, the compromise between the two crucial properties in transparent water repelling optics is clearly seen in inverse relationships as reported in TiO_2 experiments by Nkajima et al. [1]. Despite the different type of particles used in organic attachment and inorganically cured techniques, the two fabrication methods shared a close resemblance in the position of the curvature. The direct sintered samples were deposited identical particles as the inorganically cured samples. However, DS series have demonstrated a significant improvement in the efficiency of contact angle vs optical transmittance relationship. At similar optical transmissivity regions, the DS sample is capable of showing a contact angle almost 40° greater than those produced by radical bonding or sol–gel curing methods. For the purpose of this comparison, Fig. 7 illustrates the high magnification images taken with SEM. In the SEM images, it became clear that the chemical methods applied in RB and SG fabrication methods resulted in residues of excessive coupling agents. The silica particles in Fig. 7a and b appeared to be surrounded with a thick coating that reduced its overall roughness. However, in the pure physical binding technique in DS, such a problem is clearly absent in Fig. 7c. Each particle on or around agglomerate was seen as individual grains. Presumably, the reaction mechanisms behind RB and SG methods impose natural limitations to outstanding contact angles. In the organic attachment technique, the adhesion between hybrid particles and the glass substrate lays a film of soft epoxy resin. The particles directly in contact with this soft epoxy slowly embed during baking at raised temperatures. In the sol–gel curing technique, the gel suspension itself hardens into a solid film as dehydration takes place. Both of these effects eliminate the empty air space surrounding the particles. Thus, many researchers in the field that takes the sol–gel approach use a top–down technique to increase roughness in the solid film [16–21,23,26]. In contrast, directly sintered particles theoretically join at particle contact points only; this leaves a greater amount of porosity surrounding the particle structures, as shown in Fig. 4a. The intermittent porosity and particle pile-up structure result in superior surface roughness and efficiency of contact angle-optical transmittance relationship.

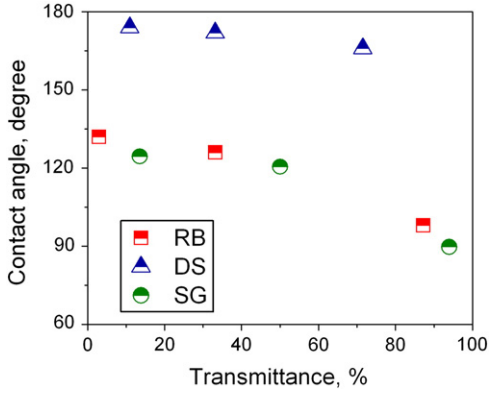

Fig. 6. Contact angles for each sample are plotted against their average optical transmittance.

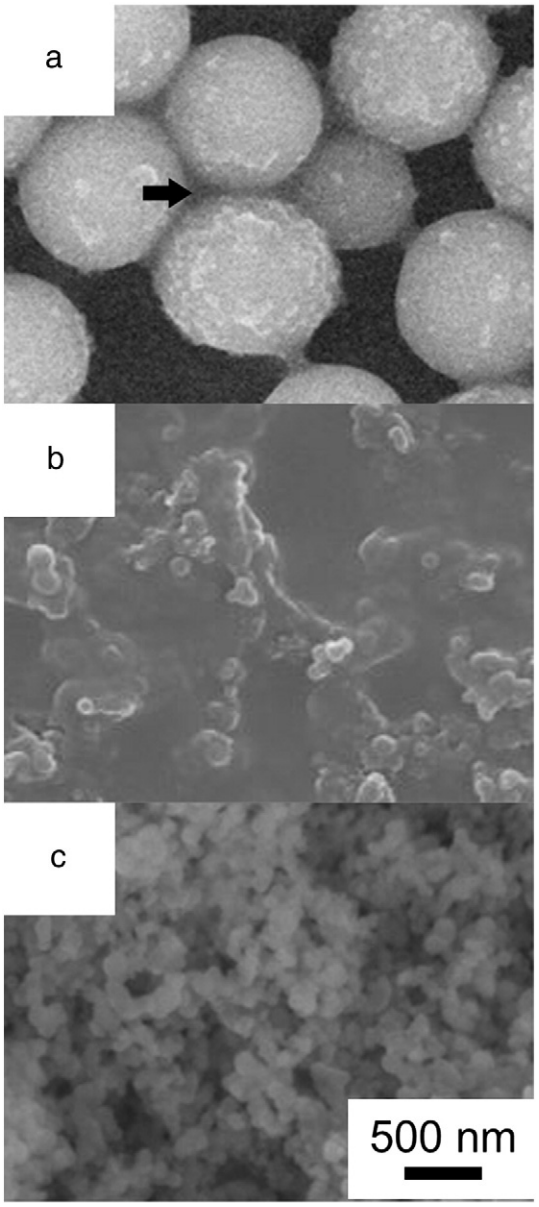

Fig. 7. High magnification images of sample surfaces on (a) RB, (b) SG, and (c) DS. Black arrow in (a) indicates the residual binder filling the voids between particles, where particles in (b) are clearly embedded in sol–gel binder.

The optimal compromise between contact angle and optical transmittance in this study was found in sample DS-1. DS-1 had a contact angle of 166° with 71% optical transmittance. The surface is well above superhydrophobic, but the average transmissivity is not adequate for optical devices. The physical binding technique is optimistic in producing 150° contact angle with greater optical transmissivity according to where the curve extends, and this was well demonstrated in a high temperature process reported by Ling et al. [2]. However, the curvature to the right of DS-1 is expected to soon experience a sharp decay as the meniscus formed on rough surface [33] structure collapses down to a contact angle with flat PDMS structure. Here, lies a challenge of transparent self-clean glazing materials. In order to reach the top right corner of the efficiency graph, the surface structure must be thin enough to avoid optical scattering whilst with the aspect ratio to sustain a surface roughness required for superhydrophobicity. Where transparency is a top priority, the choice of particle shape and method of particle deposition can be crucial to form a rough nanoscale structure. In this current comparison, the direct sintering fabrication method provides an efficient and potentially economical solution with commercially available silica powder.

3.3. Mechanical stability

All samples from three different fabrication techniques have endured 9H pencil scratch rating without additional weights added. The rating was given on the basis that the surfaces of the samples were rough structures of nano- and micro-structured protrusions, and the pencil mark would be retained if the surface structures remain attached to the glass slide. Thus, it is not able to judge the degree of surface damage given interface adhesion between the coating material and substrate surface. It is recommended an environmental simulation or long term outdoor testing to determine the deterioration of contact angle over time.

4. Conclusions

In this study, three fabrication techniques for transparent self-clean glass panels were explored, each using silicon dioxide particles to create durable surface roughness followed by a surface modification with a film of PDMS or phenyl-radical, on transparent glass substrates. Results confirmed compromise between the contact angle and optical transmittance, in inverse relationships. The optimal compromise between the contact angle and optical transmittance in this study was found in sample DS-1. DS-1 had a contact angle of 166° with 71% optical transmittance. The physical sintering technique is optimistic in producing 150° contact angle with 70%-plus optical transmissivity, more efficient than radical bonding and sol–gel sintering methods. In summary, the direct sintering fabrication method provides a potentially efficient and economical solution with commercially available silica powder for its applications.

Acknowledgements

This study was funded by the King Abdullah University of Science and Technology Global Research Partnership Award, B-04 sub plan, Advancing the Development of Solar Building Technology for the Future: KUK-C1-014-12. Further thanks to Geosciences Department, National Taiwan University for extensive uses on the FEI Quanta 200 FEG SEM; Chemical Engineering Department, National Taiwan University for extensive uses on FTA125 contact angle goniometer; and Nanomaterial and Devices Lab, and Material Science and Engineering Department, National Taiwan University for extensive uses on Ocean Optics USB2000 Fibre Optic Spectrometer.

References

[1] A. Nakajima, K. Hashimoto, T. Watanabe, K. Takai, G. Yamauchi, A. Fujishima, Langmuir 16 (2000) 7044.
[2] X.Y. Ling, I.Y. Phang, G.J. Vancso, J. Huskens, D.N. Reinhoudt, Langmuir 25 (2009) 3260.
[3] T. Yanagisawa, A. Nakajima, M. Sakai, Y. Kameshima, K. Okada, Mater. Sci. Eng. B 161 (2009) 36.
[4] Y. Paz, Z. Luo, L. Rabenberg, A. Heller, J. Mater. Res. 10 (1995) 2842.
[5] Y. Paz, A. Heller, J. Mater. Res. 12 (1997) 2759.
[6] V. Roméas, P. Pichat, C. Guillard, T. Chopin, C. Lehaut, Ind. Eng. Chem. Res. 38 (1999) 3878.
[7] Y.-Y. Lin, C.-W. Chen, W.-C. Yen, W.-F. Su, C.-H. Ku, J.-J. Wu, Appl. Phys. Lett. 92 (2008) 233301.
[8] M. Li, J. Zhai, H. Liu, Y. Song, L. Jiang, D. Zhu, J. Phys. Chem. B 107 (2003) 9954.
[9] P. Hari, M. Baumer, W.D. Tennyson, L.A. Bumm, J. Non-Cryst. Solids 354 (2008) 2843.
[10] Y. Liu, T. Tan, B. Wang, R. Zhai, X. Song, E. Li, H. Wang, H. Yan, J. Colloid Interface Sci. 320 (2007) 540.
[11] C.-H. Ku, J.-J. Wu, J. Phys. Chem. B 110 (2006) 12981.
[12] E. Hosono, S. Fujihara, I. Honma, H. Zhou, J. Am. Chem. Soc. 127 (2005) 13458.
[13] M. Ma, R.M. Hill, Curr. Opin. Colloid Interface Sci. 11 (2006) 193.
[14] J. Fresnais, J.P. Chapel, F. Poncin-Epaillard, Surf. Coat. Technol. 200 (2006) 5296.
[15] A. Tricoli, M. Righettoni, S.E. Pratsinis, Langmuir 25 (2009) 12578.

[16] N. Wang, J. Xi, S. Wang, H. Liu, L. Feng, L. Jiang, J. Colloid Interface Sci. 320 (2008) 365.
[17] Y. Li, W. Cai, B. Cao, G. Duan, F. Sun, C. Li, L. Jia, Nanotechnology 17 (2006) 238.
[18] Y. Li, W. Cai, G. Duan, B. Cao, F. Sun, F. Lu, J. Colloid Interface Sci. 287 (2005) 634.
[19] Y. Li, W. Cai, G. Duan, F. Sun, B. Cao, F. Lu, Mater. Lett. 59 (2004) 276.
[20] F. Sun, W. Cai, Y. Li, B. Cao, Y. Lei, L. Zhang, Adv. Funct. Mater. 14 (2002) 283.
[21] L. Feng, S. Li, H. Li, J. Zhai, Y. Song, L. Jiang, D. Zhu, Angew. Chem. Int. Ed. 41 (2002) 1221.
[22] C.C. Lin, S.H. Hsu, Y.L. Chang, W.F. Su, J. Mater. Chem. 20 (2010) 3084.
[23] Y. Xiu, F. Xiao, D.W. Hess, C.P. Wong, Thin Solid Films 517 (2009) 1610.
[24] Y. Xiu, D.W. Hess, C.P. Wong, J. Colloid Interface Sci. 326 (2008) 465.
[25] Y.L. Wu, Z. Chen, X.T. Zeng, Appl. Surf. Sci. 254 (2008) 6952.
[26] K.-C. Chang, Y.-K. Chen, H. Chen, Surf. Coat. Technol. 202 (2008) 3822.
[27] W. Ming, D. Wu, R. van Benthem, G. de With, Nano Lett. 5 (2005) 2298.
[28] H.M. Shang, Y. Wang, S.J. Limmer, T.P. Chou, K. Takahashi, G.Z. Cao, Thin Solid Films 472 (2005) 37.
[29] A. Schuler, J. Boudaden, P. Oelhafen, E. De Chambrier, C. Roecher, J.-L. Scartezzini, Sol. Energy Mater. Sol. Cells 89 (2005) 219.
[30] T. Soeno, K. Inokuchi, S. Shiratori, Appl. Surf. Sci. 237 (2004) 543.
[31] S. Shrinivasan, M.C. Breadmore, B. Hosticka, J.P. Landers, P.M. Norris, J. Non-Cryst. Solids 350 (2004) 391.
[32] K. Tadanaga, T. Fujii, A. Matsuda, T. Minami, M. Tatsumisago, J. Sol–Gel Sci. Technol. 31 (2004) 299.
[33] R.J. Klein, P.M. Bieshuvel, B.C. Yu, C.D. Meinhart, F.F. Lange, Z. Metallkd. 94 (2003) 377.
[34] Y. Masuda, W.S. Seo, K. Koumoto, Jpn. J. Appl. Phys. Part 1 39 (2000) 4596.
[35] Y. Masuda, M. Itoh, T. Yonezawa, K. Koumoto, Langmuir 18 (2002) 4155.
[36] H.-J. Jeong, D.-K. Kim, S.-B. Lee, S.-H. Kwon, K. Kadono, J. Colloid Interface Sci. 235 (2001) 130.
[37] D. Zhao, P. Yang, N. Melosh, J. Feng, B.F. Chmelka, G.D. Stucky, Adv. Mater. 10 (1998) 1380.
[38] L.V. Ng, A.V. McCormick, J. Phys. Chem. 100 (1996) 12517.
[39] P. Innocenzi, M.O. Abdirashid, M. Guglielmi, J. Sol–Gel Sci. Technol. 3 (1994) 47.
[40] B. D'Urso, J.T. Simpson, M. Kalyanaraman, Appl. Phys. Lett. 90 (2007) 044102.
[41] C.T. Hsieh, F.L. Wu, S.Y. Yang, Surf. Coat. Technol. 202 (2008) 6103.
[42] D.K. Sarkar, M. Farzaneh, R.W. Paynter, Mater. Lett. 62 (2008) 1226.
[43] H. Tian, X. Gao, T. Yang, D. Li, Y. Chen, J. Sol–Gel Sci. Technol. 48 (2008) 277.
[44] H. Yildirim Erbil, A. Levent Demirel, Y. Avci, O. Mert, Science 299 (2003) 1377.
[45] J. Genzer, K. Efimenko, Science 290 (2000) 2130.
[46] L. Zhai, M.C. Berg, F.C. Cebeci, Y. Kim, J.M. Milwid, M.F. Rubner, R.E. Cohen, Nano Lett. 6 (2006) 1213.
[47] M. Guo, P. Diao, S. Cai, Thin Solid Films 515 (2007) 7162.
[48] S. Yin, T. Sato, J. Mater. Chem. 15 (2005) 4584.
[49] T. Onda, S. Shibuichi, N. Satoh, K. Tsujii, Langmuir 12 (1996) 2125.
[50] Z. Cheng, L. Feng, L. Jiang, Adv. Funct. Mater. 18 (2008) 3219.
[51] J. Lee, B.H. Chu, K.-H. Chen, F. Ren, T.P. Lele, Biomaterials 30 (2009) 4488.
[52] ASTM Standard D3363-05, Standard Test Method for Film Hardness by Pencil Test, ASTM International, West Conshohocken, PA, 2005, doi:10.1520/D3363-05, www.astm.org.
[53] W. Stöber, A. Fink, E. Bohn, J. Colloid Interface Sci. 26 (1968) 62.
[54] L.C. Klein, Ann. Rev. Mater. Sci. 15 (1985) 227.